NANO LETTERS

pubs.acs.org/NanoLett Letter

Phonon Dephasing Dynamics in MoS_2

Liuyang Sun, Parveen Kumar, Zeyu Liu, Junho Choi, Bin Fang, Sebastian Roesch, Kha Tran, Joshua Casara, Eduardo Priego, Yu-Ming Chang, Galan Moody, Kevin L. Silverman, Virginia O. Lorenz, Michael Scheibner, Tengfei Luo, and Xiaoqin Li*

Cite This: *Nano Lett.* 2021, 21, 1434–1439 Read Online

ACCESS | Metrics & More | Article Recommendations | Supporting Information

ABSTRACT: A variety of quantum degrees of freedom, e.g., spins, valleys, and localized emitters, in atomically thin van der Waals materials have been proposed for quantum information applications, and they inevitably couple to phonons. Here, we directly measure the intrinsic optical phonon decoherence in monolayer and bulk MoS_2 by observing the temporal evolution of the spectral interference of Stokes photons generated by pairs of laser pulses. We find that a prominent optical phonon mode E_{2g} exhibits a room-temperature dephasing time of ~7 ps in both the monolayer and bulk. This dephasing time extends to ~20 ps in the bulk crystal at ~15 K, which is longer than previously thought possible. First-principles calculations suggest that optical phonons decay via two types of three-phonon processes, in which a pair of acoustic phonons with opposite momentum are generated.

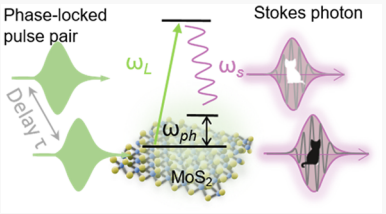

KEYWORDS: *transition metal dichalcogenides, phonon dephasing, transient coherent ultrafast phonon spectroscopy, scattering phase space*

Semiconducting van der Waals (vdW) materials, e.g., transition metal dichalcogenides (TMDCs), have emerged as a new material platform to explore various quantum degrees of freedom including spins and pseudospins (valley and layer index) for information processing.[1−3] Defect-bound single-photon emitters have been identified in TMDC monolayers and heterostructures.[4−9] Moreover, they are highly sensitive to mechanical strain,[10,11] suggesting that TMDCs are an interesting platform for studies of coupling between phonons with spins and photons in the coherent regime. To achieve this goal, one also needs to understand decoherence associated with different phonon modes. Although spontaneous Raman spectra have been routinely used to characterize layer thickness, chemical composition variations, and strain in TMDCs,[12−14] little effort has been devoted to understanding phonon coherence.

Optical phonons couple to light efficiently and subsequently decay to generate acoustic phonons. It is well-known that coherent phonons can be generated by a pulsed laser with a sufficient bandwidth, i.e. exceeding the phonon oscillation frequency[15−18] in a stimulated Raman process. However, it is not widely appreciated in the 2D material community that spontaneous Raman scattering also represents a coherent light−matter interaction process within the phonon coherence time.[19,20] This spontaneous Raman process has been used to generate the motional entanglement between vibrational states of two millimeter-sized diamonds at room temperature.[21] This scheme is just one specific example of the widely applied long-distance quantum communication protocol with linear optics.[22] To extend this approach of entangling vibrational states to new materials such as TMDCs, one needs to search for phonon modes with a long dephasing time.

In this work, we investigate intrinsic phonon dephasing dynamics in bulk and monolayer MoS_2 using a unique spectroscopy technique, transient coherent ultrafast phonon spectroscopy (TCUPS).[23] There are two commonly observed optical phonon modes, A_{1g} and E_{2g} mode in TMDCs.[12,24−30] Although stimulated Raman scattering experiments have been used to probe the coherent dynamics of the A_{1g} mode previously, the E_{2g} mode cannot be excited in those nonlinear spectroscopy experiments[31−33] because of the displacive phonon excitation mechanism and selection rules constrained by symmetry.[34] In contrast, TCUPS relies on the spontaneous Raman scattering signal generated by a pair of phase-locked laser pulses to detect the E_{2g} mode. By recording how the interference contrast decays as a function of the delay time between the two excitation pulses, our experiments reveal intrinsic phonon dephasing dynamics of the E_{2g} mode in the MoS_2 monolayer. We find that the phonon dephasing time of the E_{2g} mode is significantly longer than that of the A_{1g} mode. Our first-principles calculations suggest that the phonon dephasing involves two types of three-phonon processes in which a pair of acoustic phonons with opposite momentum are generated. The knowledge of phonon decoherence provides valuable guidance for designing phonon-photon and phonon-spin interfaces in layered materials.

Received: November 1, 2020
Revised: January 14, 2021
Published: January 28, 2021

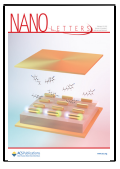

https://dx.doi.org/10.1021/acs.nanolett.0c04368
Nano Lett. 2021, 21, 1434−1439

The key concepts of TCUPS are illustrated in Figure 1. In contrast to the conventional Raman spectroscopy using a narrow-band continuous-wave (CW) laser, the excitation source used in TCUPS is a pair of phase-locked ultrafast laser pulses prepared using a Michelson interferometer as illustrated in Figure 1a (see the Supporting Information section 1 for details). The probability of each excitation laser pulse generating a Stokes-shifted photon and optical phonon is significantly less than one. If the time delay of the laser pulses is within the coherence time of the excited phonon, the time-integrated detection cannot provide information about which pulse generates the detected Stokes photon. In analogy to the double-slit experiment, the detected Raman signal is a superposition of Stokes photons generated by the laser pulse pair. This lack of "which-pulse" information leads to the interference pattern recorded in the subsingle-photon limit.[35,36]

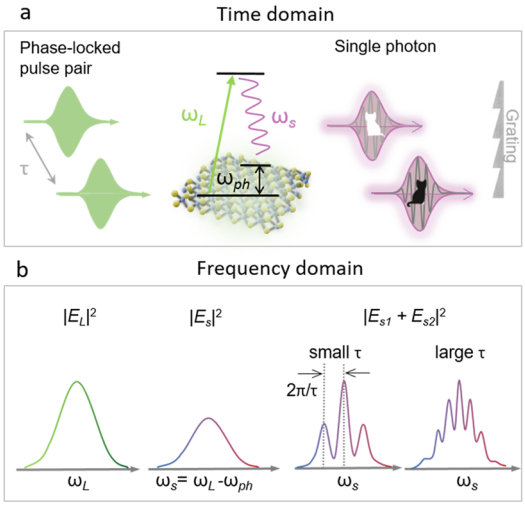

Figure 1. Illustration and concept of TCUPS. (a) Schematic of the TCUPS experiment in the time domain. A pair of phase-locked pulses excite the MoS_2 sample, and the spontaneous Raman scattering process generates Stokes photons shifted lower in energy, with the probability to generate a Stokes photon per pulse less than one statistically. In analogy to the double-slit experiment, the detected Raman signal is a superposition of Stoke photon generated by the laser pulse pair. Due to the lack of which-pulse information, the Stokes photon exhibits interference in the spectral domain, which is detected by a grating spectrometer. (b) From left to right, a schematic of the frequency-domain pulse shape of a single laser pulse, the spectrum of a Stokes signal excited by a single laser pulse, and the Stokes spectrum excited by two phase-locked laser pulses at small and large delays τ.

Following the excitation and sending the generated Stokes signal through a spectrometer, a spectrum is measured using a charge-coupled device camera, as illustrated in Figure 1b. In the frequency domain, the Stokes photons from one pulse and the incident laser pulses have very similar spectra, except that the Stokes photons are shifted toward lower energy by the phonon energy. When a Stokes photon from a pair of pulses is measured, the time-integrated interference spectrum can be written as

$$\langle |E_{\text{total}}(\omega)|^2 \rangle = |E_{S1}(\omega)|^2 + |E_{S2}(\omega)|^2 + 2\text{Re}(E_{S1}(\omega)E_{S2}^*(\omega))e^{-\Gamma|\tau|}\cos(\omega\tau) \quad (1)$$

where E_{total} is the total electric field, ω is the measured frequency, $E_{Si}(\omega)$ is the Stokes electric field ($i = 1, 2$), and τ is the time delay between the pulse pair; $\langle \ldots \rangle$ represents the shot-to-shot average, and Γ is the reverse of coherence time.[23] The interference is related to the phonon coherence due to the definite phase relation between the excitation laser, the phonon oscillations, and the Stokes photons, a feature that has been explored in a limited number of previous experiments.[19,23,35,37] As the delay τ increases, both the fringe contrast and spacing ($2\pi/\tau$) decreases, as described by $e^{-\Gamma|\tau|}$ and $\cos(\omega\tau)$ in the interference term in eq 1, illustrated in Figure 1b. The decay of the fringe contrast as a

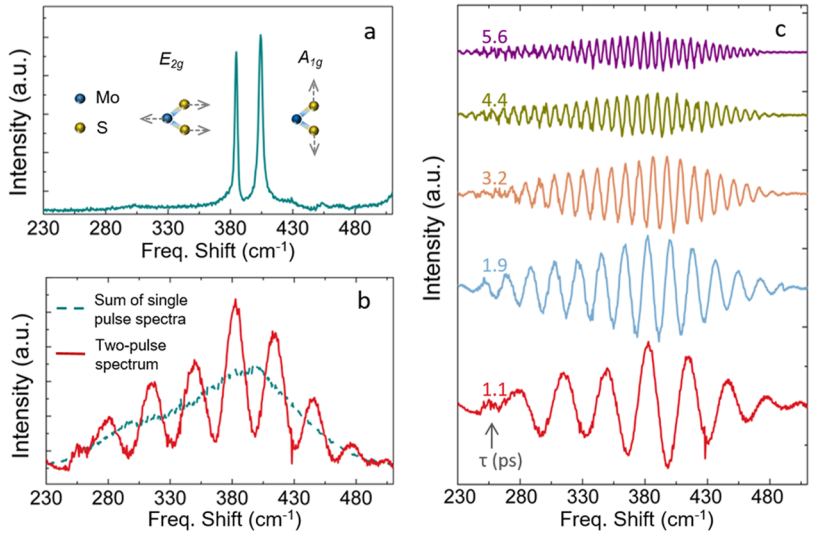

Figure 2. Raman spectra of a MoS_2 monolayer from both the conventional Raman measurement and TCUPS. (a) Conventional Raman spectrum at room temperature with excitation wavelength at 532 nm and illustrations of two common optical phonon modes, E_{2g} and A_{1g}. (b) Examples of TCUPS spectra at delay τ = 1.1 ps. The blue dashed curve is a sum of the Stokes signals recorded for each excitation pulse separately. The spectral width is determined by the excitation pulse spectrum but the center frequency is shifted from the pump by the phonon energy. This spectrum alone does not reflect the degree of coherence. Spectral interference (red solid line) appears when both excitation pulses are incident on the sample. (c) By subtracting the blue curve from the red curve in b, the interference term is isolated with the fringe visibility corresponding to the degree of coherence. The coherence lifetime is determined by varying τ.

https://dx.doi.org/10.1021/acs.nanolett.0c04368
Nano Lett. 2021, 21, 1434−1439

function of the delay can be used to extract the phonon dephasing time directly.

We first take a conventional Raman spectrum with excitation wavelength at 532 nm from a MoS_2 monolayer prepared by exfoliation method at room temperature as shown in Figure 2a. The spectrum features two prominent optical phonon modes, A_{1g} and E_{2g} modes at 404 and 384 cm^{-1}, corresponding to the out-of-plane and in-plane vibrational modes, respectively. Although the line width of the A_{1g} mode is measured as 1.85 cm^{-1}, corresponding to a phonon dephasing time 5.73 ps, the line widths of the E_{2g} mode approach the instrument response function of the spectrometer. Thus, we are unable to extract reliable information about phonon dynamics from the conventional Raman method.

TCUPS spectra from a MoS_2 monolayer are shown in Figure 2b. The blue curve is the sum of spectra generated by the pump pulses individually, i.e., $|E_{S1}(\omega)|^2 + |E_{S2}(\omega)|^2$, whereas the red curve is the interferogram observed upon excitation by a pair of phase-locked pulses. The fringe spacing $\Delta\lambda$ is determined by the delay between the two pulses and can be derived from the last term in eq 1 as $\Delta\lambda = \lambda^2/c\tau$, where $\lambda = 2\pi c/\omega$ is the free space wavelength and c is the speed of light. We tune the center wavelength of the excitation laser pulse to be 793 nm, which is below the bandgap and exciton resonance in MoS_2 to avoid exciting free carriers or electron−hole pairs. By doing so, we largely eliminate electron−phonon and exciton−phonon interaction as dephasing channels.[38−40] Thus, the phonon dephasing time measured here is mostly determined by intrinsic three-phonon processes due to the anharmonic coupling as we further discuss later. By choosing proper polarization, one can isolate either E_{2g} or A_{1g} modes or excite both modes simultaneously.[41,42] We focus on the E_{2g} mode in the current study because its longer dephasing time makes it more interesting for quantum applications. In addition, this mode is inaccessible by the ultrafast pump−probe technique.

To explore the dynamics of the E_{2g} mode and to exclude the contribution from the A_{1g} mode in the spectra, we use a linear polarizer in the detection path orthogonal to the incident laser polarization.[43−45] The A_{1g} phonon Stokes signal is thus removed because its polarization is parallel to that of the incident laser. However, the E_{2g} phonon Stokes signal is partially retained because the E_{2g} mode is doubly degenerate, with both parallel and perpendicular polarization components with respect to the incident laser polarization. We note that additional phonon modes may contribute to Raman signal when the excitation wavelength is changed to 793 nm in TCUPS measurement.[46,47] These modes either have weak intensity or have very fast dephasing rate. Thus, they have minimal contribution to the interference fringes and the extracted decay time.

The fringe contrast, or the visibility of the spectral interference, quantifies the degree of phase coherence of the excited phonon mode. A series of TCUPS spectra at various delays are taken. The interference term displayed in Figure 2c is isolated by subtracting the sum of the Stokes spectra excited by each individual pump pulse from the interferogram taken with the phase-locked pulse pair. As the time delay between the two pulses increases, the visibility of the spectral interferogram shown in Figure 2c decreases (from bottom to top), offering a direct measurement of the phonon coherence time. See SI section 3 for detailed data analysis.

We plot the amplitude of the interference term as a function of delay τ and fit the data with a single exponential function in Figure 3a (see SI section 3−4 for detailed data analysis). We

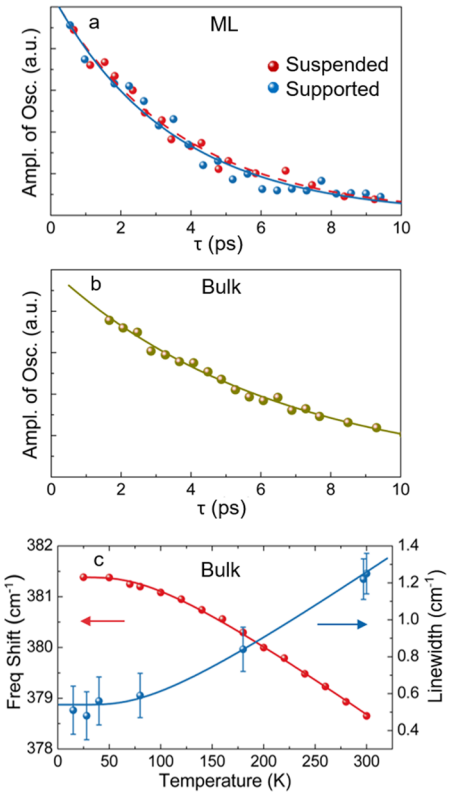

Figure 3. Measured dephasing time of the E_{2g} mode and temperature dependent studies. The amplitude of the interference term as a function of τ from both (a) a supported and suspended MoS_2 monolayer (ML) and (b) a bulk crystal. The solid lines are fittings with an exponential function. Data are taken at room temperature. The retrieved dephasing time of E_{2g} mode in monolayer and bulk MoS_2 at room temperature are 7.1 and 8.6 ps, respectively. (c) Frequency shift and line width of the E_{2g} mode in a bulk crystal as a function of temperature. Red dots are phonon frequency shifts obtained from conventional Raman spectra. Blue dots are phonon line widths obtained via TCUPS.

assume that the dephasing arises entirely from phonon population decay and that pure dephasing processes are absent. The measured coherence time is inversely proportional to the phonon line width measured in the frequency domain. Our measurements yield an E_{2g} phonon dephasing time of 7.1 ± 0.7 ps or a line width of 1.5 ± 0.1 cm^{-1} in a MoS_2 monolayer at room temperature, consistent with previous CW Raman measurements.[48,49] We repeat these measurements on both a suspended monolayer and a bulk crystal (Figure 3b). The dephasing time of the E_{2g} does not change appreciably in a suspended monolayer and increases slightly in the bulk to 8.6 ± 0.8 ps (1.3 ± 0.1 cm^{-1}) at room temperature. The similar dephasing time in these samples may originate from the nature of in-plane relative motions of the Mo and S atoms associated with the E_{2g} mode.

Having established that a monolayer and a bulk MoS_2 have similar coherence times, we focus on the temperature-dependent measurements on the bulk sample due to its better signal-to-noise ratio. In addition to a systematic temperature-dependent frequency shift of the E_{2g} mode observed by using conventional Raman spectroscopy, we also observe a systematic temperature-dependent change in phonon coherence time in TCUPS experiments, with a longer phonon dephasing time (narrower line width) 20.8 ps (0.51 cm^{-1}) at 15 K. The retrieved temperature-dependent line width from dephasing time is shown in Figure 3c. Previous Raman experiments were not able

https://dx.doi.org/10.1021/acs.nanolett.0c04368
Nano Lett. 2021, 21, 1434−1439

to capture the temperature dependence of the E_{2g} phonon line width, likely due to the limited spectral resolution (~1 cm^{-1}) of commonly accessible spectrometers. The lack of a clear temperature-dependent phonon line width was used as an evidence for impurity-scattering dominated phonon dephasing.[50] In contrast, our TCUPS experiments reveal that the dephasing time of the E_{2g} mode is significantly longer at low temperature than previously thought possible.[51] The temperature dependent frequency shifts and line widths can be well captured by Klemens model (curved lines in Figure 3c), suggesting that a three-phonon process is the leading mechanism for phonon dephasing (see SI section 5 for details).

To reveal the microscopic processes of the phonon dephasing, we further perform first-principles density functional theory (DFT) calculations of a bulk MoS_2. The calculated phonon dispersion is shown in Figure 4a. The phonon dephasing rates

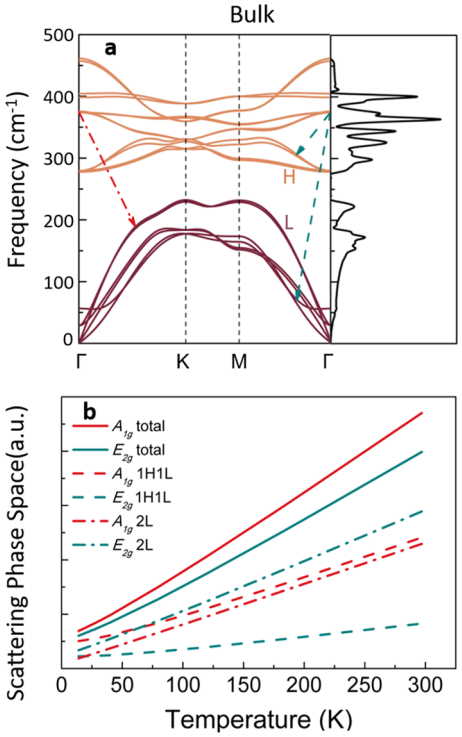

Figure 4. Calculated phonon dispersion and E_{2g} phonon scattering mechanism. (a) Phonon dispersion of a bulk MoS_2 based on first-principle calculations. Red dash-dot line and blue dashed line represent two types of decay channels for an E_{2g} phonon, i.e., 2L and 1H1L, respectively. 2L indicates both final states are low-frequency phonons below the band gap with opposite momentum. 1H1L indicates that one final state is below, whereas the other is above the band gap. Right panel shows the integrated phonon density of states. (b) Calculated contributions from the two decay channels to the total scattering phase space of the A_{1g} and E_{2g} phonon mode in a bulk MoS_2.

are determined by two factors, i.e., the availability of the scattering phase space governed by conservation rules, and the coupling strength between phonon modes characterized by anharmonicity (see details in SI section 6). Anharmonicity does not change with temperature, but the scattering phase space, where the phonon population is a factor, is temperature-dependent. As can be seen in Figure 4b, the scattering phase space increases as a function temperature, which agrees with the increasing trend of the measured line width in Figure 3c. We further divide the scattering processes into two types based on the final states: 2L and 1H1L processes. Here, the low frequency phonon modes (L) are the modes below the phonon bandgap (between 233 and 275 cm^{-1}) and the high frequency phonon modes (H) are those above this bandgap. In the 2L process (red dash-dot line in Figure 4a), one optical phonon decays into two low-frequency acoustic phonons. The 2L phonon decay process is reminiscent of the spontaneous parametric down-conversion process for the generation of correlated photon pairs via a second-order nonlinear optical process. We note that the 2L process does not necessarily require the two low-frequency phonons to have the same energy as constrained in the Klemens model. In fact, E_{2g} phonon decaying into two low-frequency phonons with the same energy is found negligible in the 2L process. In the 1H1L process (blue dashed arrow lines in Figure 4a), the E_{2g} mode decays into one high-frequency and one low-frequency phonon.

The calculated phase space in Figure 4b provides an insight into the different dephasing process between A_{1g} and E_{2g} mode. First, the smaller scattering phase space of E_{2g} mode can explain its smaller scattering rates than that of A_{1g} mode in a bulk MoS_2 at all temperatures (see temperature-dependent dephasing time of A_{1g} mode determined by conventional Raman spectroscopy in SI section 8). We note that a small phase space difference can lead to a large lifetime change.[52] In addition, the scattering phasing space indicates that the dominant decay channels for A_{1g} and E_{2g} modes are different. From Figure 4b, we see that at all temperatures, the 2L process is the dominant decay channel for the E_{2g} mode, whereas the 1H1L process is negligible. In contrast, for the A_{1g} mode, the 1H1L process contributes significantly to the overall scattering. The different decay channel between E_{2g} and A_{1g} modes is mainly due to the energy conservation rule. For the relatively low frequency E_{2g} mode in MoS_2, the number of possible H modes is very limited, and therefore, the E_{2g} mode mainly decays into two different L modes. A_{1g} mode has a higher frequency, which makes it more likely for this mode to decay through the 1H1L process.

In conclusion, by using the TCUPS method and first-principles calculation, we revealed a long dephasing time associated with the E_{2g} phonon in MoS_2. The dephasing time is measured to be ~7 ps in both a monolayer and a bulk crystal at room temperature and extends to ~21 ps at 15 K in a bulk crystal. This dephasing time is comparable to single-photon emitters identified in TMD monolayers,[4−9] suggesting phonon−exciton coupling as one of the main dephasing channels for those single-photon emitters. In addition, we show it is possible to generate collective excitations in 2D materials with lifetimes similar to that found in diamond.[23] Thus, our experiments suggest that the E_{2g} phonon can be used for generating the motional entanglement between vibrational states of two macroscopic 2D materials,[21] an interesting application in quantum information science. In the case that circularly polarized light is used, the Raman signal associated with the E_{2g} mode completely reverses the helicity of the incident photon.[41] In TMD materials, such chiral phonons at the center and corners of the honeycomb lattices may find unique applications in valleytronics.[42,53] The TCUPS technique we employ here has unique advantages in studying the coherence of all Raman-active phonon modes. Future studies may investigate the strong coupling regime between phonon−excitons or phonon−spins in vdW materials. One can envision a hybrid quantum system in vdW materials by taking advantage of coherent coupling between these degrees of freedom.

https://dx.doi.org/10.1021/acs.nanolett.0c04368
Nano Lett. 2021, 21, 1434−1439

■ ASSOCIATED CONTENT

Supporting Information

The Supporting Information is available free of charge at https://pubs.acs.org/doi/10.1021/acs.nanolett.0c04368.

Detailed experimental setup, data analysis, first-principles calculation, and conventional Raman spectroscopy measurement (PDF)

■ AUTHOR INFORMATION

Corresponding Author

Xiaoqin Li − *Department of Physics, The University of Texas at Austin, Austin, Texas 78712, United States*; Email: elaineli@physics.utexas.edu

Authors

Liuyang Sun − *Department of Physics, The University of Texas at Austin, Austin, Texas 78712, United States*; orcid.org/0000-0001-9896-4382

Parveen Kumar − *Department of Physics, University of California Merced, Merced, California 95340, United States; Stem Cell Instrumentation Foundry, University of California Merced, Merced, California 95343, United States*

Zeyu Liu − *Department of Aerospace and Mechanical Engineering, University of Notre Dame, Notre Dame, Indiana 46556, United States*

Junho Choi − *Department of Physics, The University of Texas at Austin, Austin, Texas 78712, United States*

Bin Fang − *The Center for Dynamics and Control of Materials: An NSF MRSEC, The University of Texas at Austin, Austin, Texas 78712, United States*

Sebastian Roesch − *Department of Physics, The University of Texas at Austin, Austin, Texas 78712, United States; Department of Physics, University of Tübingen, Tübingen D72076, Germany*

Kha Tran − *Department of Physics, The University of Texas at Austin, Austin, Texas 78712, United States*

Joshua Casara − *Department of Physics, University of California Merced, Merced, California 95340, United States*

Eduardo Priego − *Department of Physics, The University of Texas at Austin, Austin, Texas 78712, United States*

Yu-Ming Chang − *Center for Condensed Matter Sciences, National Taiwan University, Taipei 10617, Taiwan*

Galan Moody − *Department of Electrical and Computer Engineering, University of California Santa Barbara, Santa Barbara, California 93106, United States*

Kevin L. Silverman − *National Institute of Standards and Technology, Boulder, Colorado 80305, United States*

Virginia O. Lorenz − *Department of Physics, University of Illinois at Urbana−Champaign, Urbana, Illinois 61801, United States; IQUIST, University of Illinois at Urbana-Champaign, Urbana, Illinois 61801, United States*

Michael Scheibner − *Department of Physics, University of California Merced, Merced, California 95340, United States*

Tengfei Luo − *Department of Aerospace and Mechanical Engineering, University of Notre Dame, Notre Dame, Indiana 46556, United States*; orcid.org/0000-0003-3940-8786

Complete contact information is available at: https://pubs.acs.org/10.1021/acs.nanolett.0c04368

Author Contributions

L.S. led the TCUPS optical experiments; P.K. J.C., and B.F. led the conventional Raman experiment; Z.L. led the theoretical calculation. J.C., S.R., K.T., and E.P. prepared the MoS_2 samples; Y.C., G.M., K.S., V.O.L., M.S., T.L., and X.L. supervised the project. L.S., Z.L., T.L., and X.L. wrote the manuscript. All authors discussed the results and commented on the manuscript at all stages.

Notes

The authors declare no competing financial interest.

■ ACKNOWLEDGMENTS

We acknowledge helpful discussions with Prof. R. Merlin. The spectroscopic experiments performed at UT-Austin (J.C. and X.L.) were primarily supported by the Department of Energy, Basic Energy Science program via Grant DE-SC0019398. X.L. also acknowledges partial support from NSF DMR-1808042. Partial support for L.S. and materials preparation were provided by the Welch Foundation via Grant F-1662. B.F. and K.T. are supported by the National Science Foundation through the Center for Dynamics and Control of Materials: an NSF MRSEC under Cooperative Agreement DMR-1720595. V.O.L. acknowledges support from NSF Awards 1806572 and 1521110, and M.S. acknowledges funding by the Defense Threat Reduction Agency (Award HDTRA1-15-1-0011) and the Air Force Office of Scientific Research (Award FA9550-16-1-0278). P.K. and J.C. acknowledges funding by the Merced Nanomaterials Center for Energy and Sensing. Z.L. and T.L. thank the NSF for support from the NSF 1433490 EFRI 2DARE project. The simulations are supported by the Notre Dame Center for Research Computing and by NSF through XSEDE computing resources provided by SDSC Comet and TACC Stampede under Grant TG-CTS100078. G.M. gratefully acknowledges support via the UC Santa Barbara NSF Quantum Foundry funded via the Q-AMASE-i program under award DMR-1906325.

■ REFERENCES

(1) Geim, A. K.; Grigorieva, I. V. Van der Waals heterostructures. *Nature* **2013**, *499* (7459), 419−425.

(2) Liu, Y.; Weiss, N. O.; Duan, X.; Cheng, H.-C.; Huang, Y.; Duan, X.; et al. Van der Waals heterostructures and devices. *Nature Reviews Materials* **2016**, *1* (9), 16042.

(3) Novoselov, K. S.; et al. 2D materials and van der Waals heterostructures. *Science* **2016**, *353* (6298), No. aac9439.

(4) Grosso, G.; Moon, H.; Lienhard, B.; Ali, S.; Efetov, D. K.; Furchi, M. M.; Jarillo-Herrero, P.; Ford, M. J.; Aharonovich, I.; Englund, D.; et al. Tunable and high-purity room temperature single-photon emission from atomic defects in hexagonal boron nitride. *Nat. Commun.* **2017**, *8* (1), 705.

(5) Srivastava, A.; et al. Optically active quantum dots in monolayer WSe2. *Nat. Nanotechnol.* **2015**, *10* (6), 491−496.

(6) Koperski, M.; et al. Single photon emitters in exfoliated WSe2 structures. *Nat. Nanotechnol.* **2015**, *10* (6), 503−506.

(7) He, Y.-M.; et al. Single quantum emitters in monolayer semiconductors. *Nat. Nanotechnol.* **2015**, *10* (6), 497−502.

(8) Chakraborty, C.; et al. Voltage-controlled quantum light from an atomically thin semiconductor. *Nat. Nanotechnol.* **2015**, *10* (6), 507−511.

(9) Tonndorf, P.; et al. Single-photon emission from localized excitons in an atomically thin semiconductor. *Optica* **2015**, *2* (4), 347−352.

(10) Aslan, O. B.; Deng, M.; Heinz, T. F. Strain tuning of excitons in monolayer ${\mathrm{WSe}}_{2}$. *Phys. Rev. B: Condens. Matter Mater. Phys.* **2018**, *98* (11), 115308.

(11) Lloyd, D.; et al. Band Gap Engineering with Ultralarge Biaxial Strains in Suspended Monolayer MoS2. *Nano Lett.* **2016**, *16* (9), 5836−5841.

(12) Li, H.; et al. From bulk to monolayer MoS2: evolution of Raman scattering. *Adv. Funct. Mater.* **2012**, *22* (7), 1385−1390.

(13) Lu, X.; et al. Lattice vibrations and Raman scattering in two-dimensional layered materials beyond graphene. *Nano Res.* **2016**, *9* (12), 3559−3597.
(14) Zhao, Y.; et al. Interlayer Breathing and Shear Modes in Few-Trilayer MoS2 and WSe2. *Nano Lett.* **2013**, *13* (3), 1007−1015.
(15) Yan, Y.-X.; Gamble, E. B.; Nelson, K. A. Impulsive stimulated scattering: General importance in femtosecond laser pulse interactions with matter, and spectroscopic applications. *J. Chem. Phys.* **1985**, *83* (11), 5391−5399.
(16) Merlin, R. Generating coherent THz phonons with light pulses. *Solid State Commun.* **1997**, *102* (2), 207−220.
(17) Randi, F.; et al. Probing the Fluctuations of Optical Properties in Time-Resolved Spectroscopy. *Phys. Rev. Lett.* **2017**, *119* (18), 187403.
(18) Glerean, F.; et al. Quantum model for impulsive stimulated Raman scattering. *J. Phys. B: At., Mol. Opt. Phys.* **2019**, *52* (14), 145502.
(19) Fazio, B.; et al. Coherent backscattering of Raman light. *Nat. Photonics* **2017**, *11* (3), 170−176.
(20) Shinbrough, K.; et al. Photon-matter quantum correlations in spontaneous Raman scattering. *Phys. Rev. A: At., Mol., Opt. Phys.* **2020**, *101* (1), 013415.
(21) Lee, K. C.; et al. Entangling Macroscopic Diamonds at Room Temperature. *Science* **2011**, *334* (6060), 1253−1256.
(22) Duan, L. M.; et al. Long-distance quantum communication with atomic ensembles and linear optics. *Nature* **2001**, *414* (6862), 413−418.
(23) Waldermann, F. C.; et al. Measuring phonon dephasing with ultrafast pulses using Raman spectral interference. *Phys. Rev. B: Condens. Matter Mater. Phys.* **2008**, *78* (15), 155201.
(24) Lee, C.; et al. Anomalous lattice vibrations of single-and few-layer MoS2. *ACS Nano* **2010**, *4* (5), 2695−2700.
(25) Zhang, X.; et al. Phonon and Raman scattering of two-dimensional transition metal dichalcogenides from monolayer, multilayer to bulk material. *Chem. Soc. Rev.* **2015**, *44* (9), 2757−2785.
(26) Chakraborty, B.; et al. Layer-dependent resonant Raman scattering of a few layer MoS2. *J. Raman Spectrosc.* **2013**, *44* (1), 92−96.
(27) Sahoo, S.; et al. Temperature-Dependent Raman Studies and Thermal Conductivity of Few-Layer MoS2. *J. Phys. Chem. C* **2013**, *117* (17), 9042−9047.
(28) Taube, A.; et al. Temperature-dependent nonlinear phonon shifts in a supported MoS2 monolayer. *ACS Appl. Mater. Interfaces* **2014**, *6* (12), 8959−63.
(29) Ridley, B. The electron-phonon interaction in quasi-two-dimensional semiconductor quantum-well structures. *J. Phys. C: Solid State Phys.* **1982**, *15* (28), 5899.
(30) Li, W.; Carrete, J.; Mingo, N. Thermal conductivity and phonon linewidths of monolayer MoS2 from first principles. *Appl. Phys. Lett.* **2013**, *103* (25), 253103.
(31) Trovatello, C.; et al. Strongly Coupled Coherent Phonons in Single-Layer MoS2. *ACS Nano* **2020**, *14* (5), 5700−5710.
(32) Jeong, T. Y.; et al. Coherent Lattice Vibrations in Mono- and Few-Layer WSe2. *ACS Nano* **2016**, *10* (5), 5560−5566.
(33) He, B.; Zhang, C.; Zhu, W.; Li, Y.; Liu, S.; Zhu, X.; Wu, X.; Wang, X.; Wen, H.-h.; Xiao, M.; et al. Coherent optical phonon oscillation and possible electronic softening in WTe2 crystals. *Sci. Rep.* **2016**, *6* (1), 30487.
(34) Zeiger, H. J.; et al. Theory for displacive excitation of coherent phonons. *Phys. Rev. B: Condens. Matter Mater. Phys.* **1992**, *45* (2), 768−778.
(35) Meiselman, S.; et al. Observation of coherence oscillations of single ensemble excitations in methanol. *J. Opt. Soc. Am. B* **2014**, *31* (9), 2131−2135.
(36) Rangarajan, R.; Goggin, M.; Kwiat, P. Optimizing type-I polarization-entangled photons. *Opt. Express* **2009**, *17* (21), 18920−18933.
(37) Lee, K.; et al. Comparing phonon dephasing lifetimes in diamond using transient coherent ultrafast phonon spectroscopy. *Diamond Relat. Mater.* **2010**, *19* (10), 1289−1295.
(38) Carvalho, B. R.; et al. Symmetry-dependent exciton-phonon coupling in 2D and bulk MoS2 observed by resonance Raman scattering. *Phys. Rev. Lett.* **2015**, *114* (13), 136403.
(39) Song, Y.; Dery, H. Transport theory of monolayer transition-metal dichalcogenides through symmetry. *Phys. Rev. Lett.* **2013**, *111* (2), 026601.
(40) Carvalho, B. R.; Wang, Y.; Mignuzzi, S.; Roy, D.; Terrones, M.; Fantini, C.; Crespi, V. H.; Malard, L. M.; Pimenta, M. A.; et al. Intervalley scattering by acoustic phonons in two-dimensional MoS2 revealed by double-resonance Raman spectroscopy. *Nat. Commun.* **2017**, *8*, 14670.
(41) Chen, S.-Y.; et al. Helicity-resolved Raman scattering of MoS2, MoSe2, WS2, and WSe2 atomic layers. *Nano Lett.* **2015**, *15* (4), 2526−2532.
(42) Zhang, L.; Niu, Q. Chiral Phonons at High-Symmetry Points in Monolayer Hexagonal Lattices. *Phys. Rev. Lett.* **2015**, *115* (11), 115502.
(43) Doratotaj, D.; Simpson, J. R.; Yan, J.-A. Probing the uniaxial strains in MoS 2 using polarized Raman spectroscopy: A first-principles study. *Phys. Rev. B: Condens. Matter Mater. Phys.* **2016**, *93* (7), 075401.
(44) Wang, Y.; et al. Raman Spectroscopy Study of Lattice Vibration and Crystallographic Orientation of Monolayer MoS2 under Uniaxial Strain. *Small* **2013**, *9* (17), 2857−2861.
(45) Liang, L.; Meunier, V. First-principles Raman spectra of MoS2, WS2 and their heterostructures. *Nanoscale* **2014**, *6* (10), 5394−5401.
(46) Placidi, M.; et al. Multiwavelength excitation Raman scattering analysis of bulk and two-dimensional MoS 2: vibrational properties of atomically thin MoS 2 layers. *2D Mater.* **2015**, *2* (3), 035006.
(47) Lee, J.-U.; et al. Anomalous excitonic resonance Raman effects in few-layered MoS 2. *Nanoscale* **2015**, *7* (7), 3229−3236.
(48) Hase, M.; et al. Dynamics of coherent phonons in bismuth generated by ultrashort laser pulses. *Phys. Rev. B: Condens. Matter Mater. Phys.* **1998**, *58* (9), 5448.
(49) Califano, S.; Schettino, V. Vibrational relaxation in molecular crystals. *Int. Rev. Phys. Chem.* **1988**, *7* (1), 19−57.
(50) Taube, A.; et al. Temperature-Dependent Nonlinear Phonon Shifts in a Supported MoS2Monolayer. *ACS Appl. Mater. Interfaces* **2014**, *6* (12), 8959−8963.
(51) Anees, P.; Valsakumar, M. C.; Panigrahi, B. K. Anharmonicity of optic modes in monolayer MoS2. *Appl. Phys. Lett.* **2016**, *108* (10), 101902.
(52) Liu, Z.; Wu, X.; Luo, T. The impact of hydrogenation on the thermal transport of silicene. *2D Mater.* **2017**, *4* (2), 025002.
(53) Zhu, H.; et al. Observation of chiral phonons. *Science* **2018**, *359* (6375), 579−582.

https://dx.doi.org/10.1021/acs.nanolett.0c04368
Nano Lett. 2021, 21, 1434−1439